Theoretical study of isoelectronic Si_nM clusters ($M=Sc^-, Ti, V^+$; $n=14-18$)

M. B. Torres*
Departamento de Matemáticas y Computación, Universidad de Burgos, 09006 Burgos, Spain

E. M. Fernández†
Center for Atomic-Scale Materials Design, Department of Physics, Building 307, Technical University of Denmark, DK-2800 Lyngby, Denmark

L. C. Balbás‡
Departamento de Física Teórica, Universidad de Valladolid, E-47011 Valladolid, Spain

(Received 2 January 2007; revised manuscript received 12 April 2007; published 16 May 2007)

We study, from first-principles quantum mechanical calculations, the structural and electronic properties of several low-lying energy equilibrium structures of isoelectronic Si_nM clusters ($M=Sc^-, Ti, V^+$) for $n=14-18$. The main result is that those clusters with $n=16$ are more stable than its neighbors, in agreement with recent experimental mass spectra. By analyzing the orbital charge distribution and the partial orbital density of states, that special stability is rationalized as a combination of geometrical (near spherical cagelike structure for $n=16$) and electronic effects (*l-selection rule* of the spherical potential model). The structures of the two lowest energy isomers of $Si_{16}M$ are nearly degenerate, and consist of the Frank-Kasper polyhedron and a distortion of that polyhedron. The first structure is the ground state for $M=V^+$, and the second is the ground state for Ti and Sc^-. For the lowest energy isomers of clusters Si_nM with $n=14-18$, we analyze the changes with size n, and impurity M of several quantities: binding energy, second difference of total energy, HOMO-LUMO gap, adiabatic electron affinity, addition energy of a Si atom, and addition energy of an M impurity to a pure Si_n cluster. We obtain good agreement with available measured adiabatic electron affinities for Si_nTi.

DOI: 10.1103/PhysRevB.75.205425 PACS number(s): 36.40.Cg, 36.40.Qv

I. INTRODUCTION

Promising applications of silicon nanoclusters, both pure[1] and doped with transition-metal atoms,[2] have originated many studies and raised interesting questions about their electronic and structural properties. Pure Si_n clusters, as inferred from experimental measurements,[3–6] are prolate for $n<27$ and became near spherical for $n>27$, which has been corroborated by computational studies.[1,7–15] On the other hand, the growth behavior of transition-metal-doped silicon clusters seems to follow a different pattern than pure Si clusters. There are several calculations of Si_nM structures for various cluster sizes and impurity atoms or ions.[16–25] Kumar and co-workers[17,18] have found that open basketlike structures are the most favorable for $n=8-12$, while for $n=13-16$ the metal atom is completely surrounded by Si atoms. The optimal cage for many of the metal-encapsulated silicon clusters,[2,16] occurs at $n=16$. These predictions were later confirmed indirectly by experiments. Thus, experiments on photodissociation of MSi_n clusters[26] indicate that, for $M=Cr$, encapsulation of Cr occurs at $n=15-16$. A mass spectrometric stability study of binary MS_n clusters,[27] with $S=Si, Ge, Sn, Pb$, and $M=Cr, Mn, Cu, Zn$, reveals interesting trends. For example, Cr-doped silicon cationic clusters are peculiarly abundant at sizes $n=15$ and 16, as already obtained by Beck twenty years ago.[28,29] Other experiments, combining mass spectrometry, a chemical probe method, and photoelectron spectroscopy,[30] revealed that one metal atom ($M=Ti, Hf, Mo, W$) can be encapsulated inside a Si_n cage at $n\geq 15$. In recent mass spectrometry experiments, Nakajima and co-workers[31] have shown the size-selective formation of $Si_{16}Sc^-$, $Si_{16}Ti$, and $Si_{16}V^+$ clusters. More details about these experiments, combining mass spectrometry, anion photoelectron spectroscopy, and adsorption reactivity towards H_2O, have been published very recently.[32]

Concerning the special stability of $Si_{16}M$ for the type of M impurity involved in the experiments of Nakajima and co-workers,[31] we have found very few works.[16,33,34] Kumar and Kawazoe[16] obtained for $Si_{16}Ti$ a truncated tetrahedral structure, called the Frank-Kasper (FK) polyhedron. In further works (see Ref. 2 for a review), Kumar and co-workers explained the special stability of that cluster in terms of the spherical potential model,[35–37] as a combination of geometrical and electronic shell effects. In the work of Reveles and Khana,[33] cationic, neutral, and anionic doped clusters Si_nM with $n=15-17$, were optimized. These authors obtained that $Si_{16}M$ clusters with $M=Sc^-, Ti, V^+$, adopt the FK-polyhedron structure in their ground state, having the highest occupied molecular orbital-lowest unoccupied molecular orbital (HOMO-LUMO) Gap and the atomization energy larger than the same clusters within other charge states, which is a manifestation of stability against changes in the electronic charge. The explanation of this fact was based on a *20 electron rule*, assuming that only one electron is contributed by a Si atom to the valence manifold when that Si atom is bonded to the metal atom.

We have studied recently[34] Si_nSc^- clusters in the range n=14–18, resulting at $n=16$ a positive peak for the second difference in the total energy [see Eq. (4)], which is related directly to the higher abundance of that cluster in the mass spectrometry experiment.[31] In order to explain these experiments for $M=Ti$ and V^+, and to reveal the roll of the impurity, we have performed in the present work systematic stud-

ies of the relative stability of Si_n and Si_nM for $n=14-18$ and $M=$ Sc^-, Ti, and V^+. We find that for $n=16$ these doped clusters are more stable than its neighbors clusters, in agreement with the experiments.[31,32] In the course of searching for equilibrium geometries we have found a new lowest energy isomer of $Si_{16}Sc^-$ which is nearly degenerate with the one reported in our preliminary work.[34]

In addition to geometries and stability, we have studied other properties of Si_nM clusters. For these doped clusters, we will compare the binding (atomization) energy per atom,

$$E_b(\mathrm{Si}_n M) = [E(M) + nE(\mathrm{Si}) - E_n(\mathrm{Si}_n M)]/(n+1), \quad (1)$$

the addition energy of an M impurity to a Si_n cluster,

$$E_{ad}^{M}(\mathrm{Si}_n M) = E(\mathrm{Si}_n) + E(M) - E_n(\mathrm{Si}_n M), \quad (2)$$

the addition energy of a Si atom to a $Si_{n-1}M$ cluster,

$$E_{ad}^{\mathrm{Si}}(\mathrm{Si}_n M) = E(\mathrm{Si}_{n-1} M) + E(\mathrm{Si}) - E_n(\mathrm{Si}_n M), \quad (3)$$

the second difference of the cluster energy,

$$\Delta_2 E_n(\mathrm{Si}_n M) = E(\mathrm{Si}_{n+1} M) + E(\mathrm{Si}_{n-1} M) - 2E(\mathrm{Si}_n M), \quad (4)$$

and the energy difference between the eigenvalues of the lowest unoccupied (LUMO) and the highest occupied (HOMO) molecular orbital, Δ_n^{gap}. In the expressions above $E(X)$ is the total energy of system X. The second difference energy $\Delta_2 E_n$ is equivalent to $E_{ad}^{\mathrm{Si}}(Si_nM) - E_{ad}^{\mathrm{Si}}(\mathrm{Si}_{n+1}M)$. This second difference is proportional to $\log(I_n/I_{n+1})$, where I_n is the intensity of the Si_nM signal in the experimental mass spectra.[38] In order to compare with existing experimental values, we calculated the adiabatic electron affinity of neutral Si_nSc, Si_nTi, and Si_nV. To do that, we have also optimized the structures of Si_nSc, Si_nTi^-, Si_nV, and Si_nV^- starting with several low-lying energy isomers of conveniently charged Si_nM clusters.

In Sec. II we outline briefly the computational method. In Sec. III we present and discuss the results. Firstly, in Sec. III A we present the geometrical structures of several low-lying isomers, which are compared to previous results. In Sec. III B we discuss the electronic energy trends of the lowest energy isomer of Si_nSc^-, Si_nTi, and Si_nV^+ clusters. Conclusions of this study are given in Sec. IV.

II. COMPUTATIONAL PROCEDURE

We have used the density functional theory[39] (DFT) code SIESTA[40] within the generalized gradient approximation as parametrized by Perdew, Burke, and Ernzerhof[41] for the exchange-correlation effects. Details about the pseudopotentials and basis sets are the same as in our previous work.[34] Specifically, we used norm conserving scalar relativistic pseudopotentials[42] in their fully nonlocal form,[43] generated from the atomic valence configuration $3s^23p^2$ for Si (with core radii 1.9 a.u. for s and p orbitals), and the semicore valence configuration $4s^23p^63d^n$ for Sc ($n=1$), Ti ($n=2$), and V ($n=3$) (all of them with core radii, in a.u., 2.57, 1.08, and 1.37 for s, p, and d orbitals, respectively). In the present calculations we used a double-ζ basis s,p (for Si) and s,p,d (for M), with single polarization d (for Si) and p for M, having maximum cutoff radius, in a.u., 7.47 (Si), 8.85 (Sc), 8.45 (Ti), and 8.08 (V). The basis set and pseudopotentials of M atoms were used and tested before in Refs. 44 and 45. The grid fineness is controlled by the energy cutoff of the plane waves that can be represented in it without aliasing (120 Ry in this work).

As a further test of the pseudopotentials, basis sets, and cutoff energy, we have calculated the relative stability, bond distance, and dipole moment of different spin states of SiM^{ν} monosilicides ($M=Sc^-,Ti,V^+$; $\nu=\pm1,0$), and compared these values with those calculated recently by Wu and Su[46] using a standard all-electron density functional method. In all cases the spin multiplicity of the lower energy state is the same as in the Wu and Su calculations. Specifically, we obtained a triplet state for $SiSc^-$ and a quintuplet for SiTi and SiV^+, with bond distances 2.50, 2.51, and 2.51 Å, respectively, to be compared with the values 2.43, 2.45, and 2.50 Å, respectively, obtained by Wu and Su.[46] The calculated electric dipole moments for the neutral species are, in Debye, 3.17 D (SiSc quadruplet), 3.36 D (SiTi quintuplet), and 3.13 D (SiV sextuplet), to be compared with the values 3.62, 3.58, and 3.20 D, respectively, reported by Wu and Su.[46]

The equilibrium geometries result from an unconstrained conjugate-gradient structural relaxation using the DFT forces. We try out several initial structures for each cluster (typically more than twenty) until the force on each atom was smaller than 0.010 eV/Å. These initial geometries were constructed from previous works,[18,17,19] from our optimized geometries[34] of neutral Si_n with a Sc^-, Ti, or V^+ atom added at different sites, and from many other configurations that we have invented.

In order to identify the isomers of a particular Si_nM cluster, we have ordered the isomers according to their energy difference with the lowest energy one and labeled clusters 1, 2, 3,…starting with the ground state. This number we refer to later as the ordinal number of the isomer.

III. RESULTS AND DISCUSSIONS

A. Geometry of Si_nM doped clusters ($M=Sc^-,Ti,V^+$; $n=14-18$)

The equilibrium geometry of a few low-lying energy isomers of isoelectronic Si_nM doped clusters ($M=Sc^-,Ti,V^+$) is represented in Figs. 1–5 for the sizes $n=14-18$, respectively. In all these structures the M impurity is surrounded by Si atoms. For each structure and type of impurity (M) are given the total energy difference with respect to the lowest energy isomer, the HOMO-LUMO gap, and the ordinal number for that isomer, which was described earlier in Sec. II. Most structures are common to the three types of impurity, but the ordinal of the isomer changes in several cases from an impurity to the other. Specifically, the structure of the first isomer is the same for all Si_nM clusters, except for Si_nV^+ with $n=16-18$. The first isomer of Si_nV^+, for $n=16,17$, is the second isomer of Si_nM ($M=Sc^-,Ti$). In general, the structure of the third, and higher, isomers of Si_nV^+ and Si_nTi depart from the sequence for Si_nSc^-. On the other hand, there is no relation between the structures of Si_nM in Figs. 1–5 and

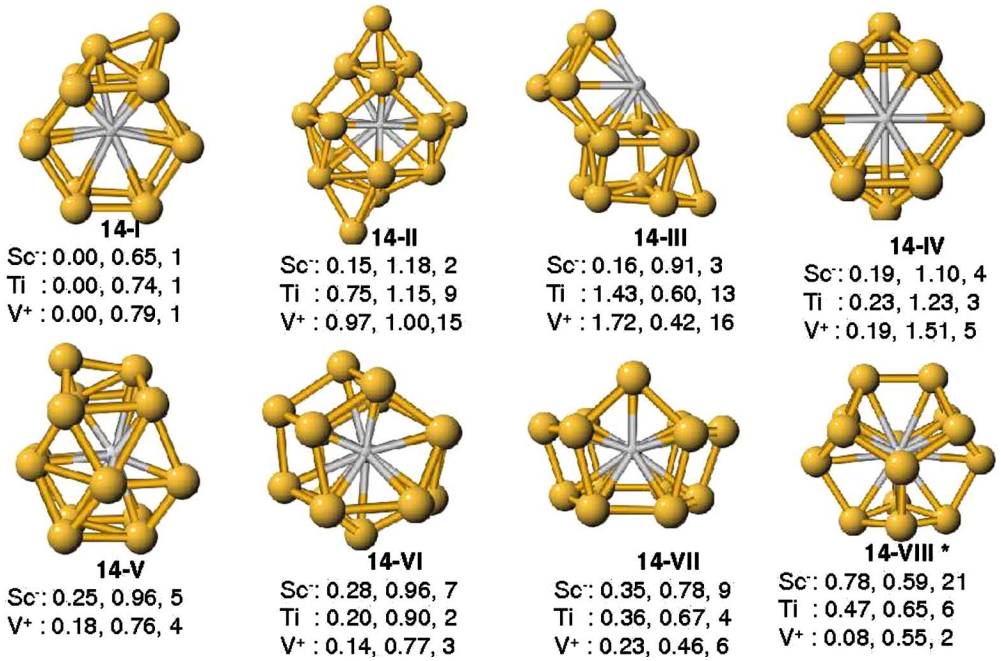

FIG. 1. (Color online) Geometry of the few lowest energy isomers of $Si_{14}M$ clusters. The index I in the label 14-I indicates the different geometries. Below each structure is given, for the three different types of dopant, the total energy difference with respect to the lowest energy configuration (eV), the HOMO-LUMO gap (eV), and the ordinal number of the isomer. In all structures the spin state is a singlet except for 14-VIII* which is a triplet (indicated by an asterisk).

those of Si_n or Si_{n+1} obtained in our previous work.[34]

A common structural motif for the ground state structure of Si_nM with $n=14,17,18$, is a distorted hexagonal prism (DHP) of Si atoms surrounding the M impurity, with additional Si atoms and dimers decorating the lateral prism faces.[34] That DHP motif resembles the structures C_s (ground state) and C_{2h} reported recently for $Si_{12}Ni$.[20] That structure C_s has been found as the new ground state of $Si_{12}Ni$, instead of the C_{5v} symmetric Frank-Kasper structure, which was believed the lowest energy isomer, but it is unstable.

Similarly to the case of pure Si_n clusters discussed by Hellmann and co-workers[13] and in previous works,[9–11,34] several isomers of doped Si_nM clusters are found in a narrow energy interval. The determination of the ground state geometry is then a difficult task, and calculated properties which are not directly related to the total energy will be averaged with adequate weights in order to check against experimental determinations at finite temperature.[13]

In Table I are given the average bond distances Si-M and Si-Si for several isomers of Si_nM clusters. These distances are smaller for $Si_{16}M$ and $Si_{15}M$ clusters, and, for a given size n, the distance Si-M decreases smoothly from Si_nSc^- to Si_nTi to Si_nV^+, following the same tendency as the metallic bond radius of the atomic impurities, namely 1.63, 1.45, and

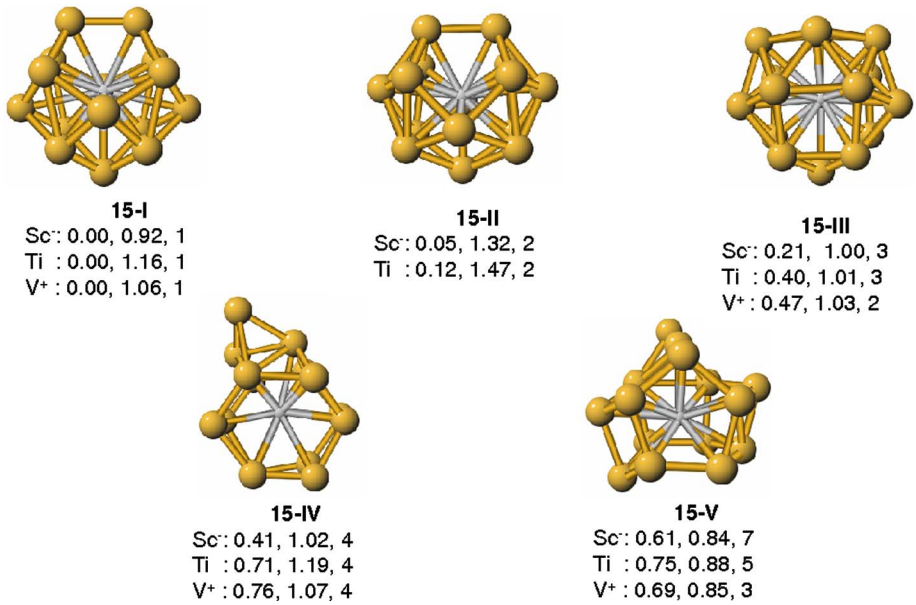

FIG. 2. (Color online) Same as Fig. 1 for $n=15$.

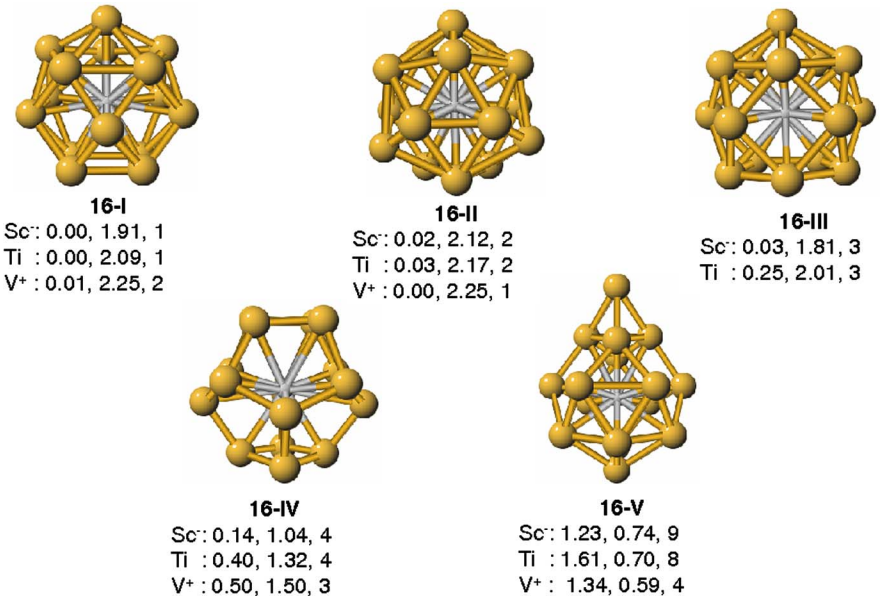

FIG. 3. (Color online) Same as Fig. 1 for $n=16$. The structure 16-III is not stable for $Si_{16}V^+$, and evolves towards structure 16-II (see text).

1.31 Å for Sc, Ti, and V, respectively.[47] The state of charge also has influence on the overall size of these clusters, as noted by Koyasu *et al.*,[32] being the anions larger than the cations. There are two or more maxima in the distributions of Si-*M* distances, depending on the isomeric geometry. For example, the maxima of $d_{av}^{\text{Si-}M}$ for the isomers 16-I to 16-IV of $Si_{16}M$ are indicated in Fig. 7, and correspond to well defined radial shells of Si atoms around the central *M* impurity. Thus, for the isomer 16-II (FK geometry) there are two atomic shells composed of 4 and 12 Si atoms, respectively, the first shell forming a perfect tetrahedron. It is interesting to note that the electronic charge distribution of a perfect tetrahedral molecule X_4 have zero dipole and quadrupole electric moments, and then behaves approximately as a spherical charge distribution.

The average Si-Si distance is also smaller for $Si_{16}M$ and $Si_{15}M$ clusters, and, for a given size and structure, is smaller for Si_nV^+ than Si_nTi and than Si_nSc^- clusters. The distribution of Si-Si distances shows two maxima for $n \leqslant 16$, at about (roughly) 2.5 and 4.5 Å which are larger than the first and second neighbor Si-Si distances in bulk Si, respectively. In some cases there are three maxima, like in the 14-VIII isomer [the only structure which prefers spin triplet instead of spin singlet multiplicity (see below Sec. III A 1)], or the fullerene type 16-IV isomer, with maxima at about 2.5, 3.8, and 5.1 Å, in both cases. For $n=17,18$ isomers there is only one broad maximum in the Si-Si distance distributions.

1. $Si_{14}M$ ($M=Sc^-, Ti, V^+$)

The structure of several low energy isomers of $Si_{14}M$ clusters are represented in Fig. 1. For the first isomer of $Si_{14}M$ we obtain a DHP structure decorated with a Si_2 dimer on a side. That structure is similar to the first isomer of $ZrSi_{14}$ found by Lu and Nagase,[21] and to the second isomer of $ZrSi_{14}$ found by Wang and Han.[19] The second, third, and fourth isomers of $Si_{14}Sc^-$, with structures 14-II, 14-III, and

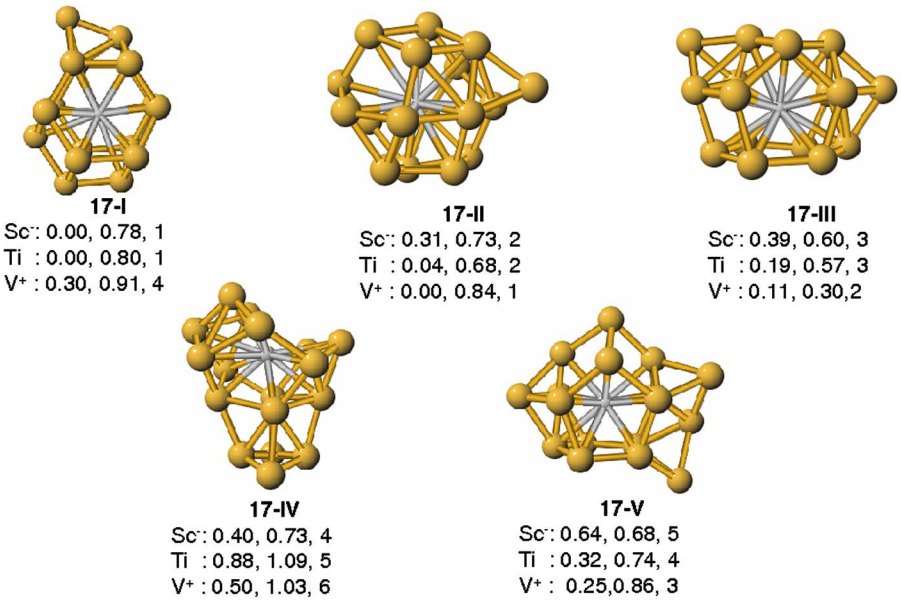

FIG. 4. (Color online) Same as Fig. 1 for $n=17$.

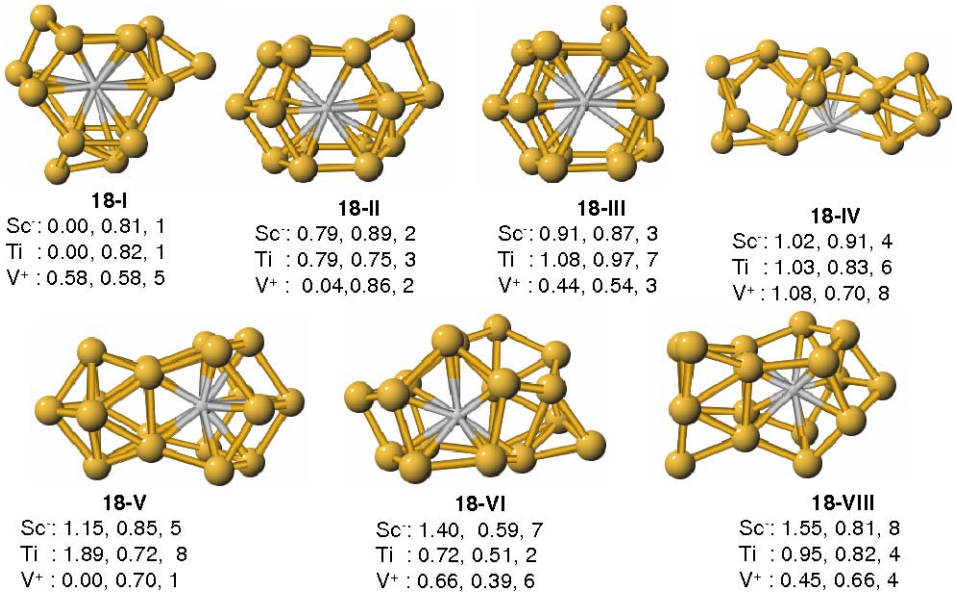

FIG. 5. (Color online) Same as Fig. 1 for $n=18$.

14-IV, respectively, were obtained by Torres *et al.*[34] Not among these structures is the one for the second isomer of $Si_{14}Ti$ or $Si_{14}V^+$, but 14-IV is adopted by the third isomer of $Si_{14}Ti$, and the fifth isomer of $Si_{14}V^+$.

The structure of the second isomer of $Si_{14}Ti$ (14-VI) is similar to the third isomer of $Si_{14}V^+$ and the seventh isomer of $Si_{14}Sc^-$. The structure of the fourth isomer of $Si_{14}Ti$, which is similar to the ninth isomer of $Si_{14}Sc^-$, was obtained by Kawamura *et al.*[17] as the fifth isomer of $Si_{14}Cr$, and by Wang and Han[19] as the first isomer of $Si_{14}Zr$.

The structure of the second isomer of $Si_{14}V^+$ (14-VIII) is shared with the sixth isomer of $Si_{14}Ti$ and the 21st of $Si_{14}Sc^-$, and deserves special attention because it is the only case whose spin multiplicity is a triplet (see below, Sec. III B 2). The triplet-singlet energy difference for the optimized structure 14-VIII of $Si_{14}M$ is 0.05, 0.18, and 0.42 eV for $M=Sc^-$, Ti, and V^+, respectively. The structure 14-VIII resembles the second isomer of $Si_{14}Ti$ given by Kawamura *et al.*[18] The structure 14-V, which is adopted by the fourth isomer of $Si_{14}V^+$ and the fifth of $Si_{14}Sc^-$, is not found among the low-lying energy isomers of $Si_{14}Ti$.

We have tested other structures of $Si_{14}Ti$ given in the literature.[17,18] Thus, the first isomer of $Si_{14}Ti$ reported by Kawamura *et al.*[18] corresponds to our twelfth, seventh, and ninth isomers for Sc^-, Ti, and V^+ impurities, respectively, with the energy difference 0.57, 0.53, and 0.39 eV, and spin zero. When we optimize that structure for the triplet spin state, there results a triplet-singlet energy difference of 0.62, 0.74, and 0.62 eV for $M=Sc^-$, Ti, and V^+, respectively. Similarly, the structure of the first isomer of $Si_{14}Ti$ reported by Kawamura *et al.*[17] corresponds to our isomers 16th, 10th, and 11th of $Si_{14}M$, with energy difference (with respect to the ground state) 0.63, 0.76, and 0.68 eV, and triplet-singlet energy difference 0.27, 0.10, and 0.09 eV, for $M=Sc^-$, Ti, and V^+, respectively. Finally, the cubic structure reported for the ground state of $Si_{14}Fe$,[16,22] corresponds to our 27th, 12th,

TABLE I. Average distances, in Å, d_{av}(M-Si) and d_{av}(Si-Si), including their standard deviation, for several low-lying isomers of Si_nM clusters, labeled in the first column as in Figs. 1–5.

	d_{av}(Si-M)			d_{av}(Si-Si)		
	Si_nSc^-	Si_nTi	Si_nV^+	Si_nSc^-	Si_nTi	Si_nV^+
14-I	2.91±0.29	2.87±0.29	2.85±0.30	4.11±1.19	4.06±1.17	4.03±1.16
14-VIII	2.85±0.08	2.82±0.05	2.80±0.05	4.05±1.10	3.99±1.08	3.97±1.07
15-I	2.85±0.11	2.82±0.11	2.80±0.11	4.02±1.10	3.97±1.09	3.94±1.08
16-I	2.87±0.08	2.83±0.10	2.81±0.11	4.04±1.11	3.99±1.10	3.97±1.10
16-II	2.87±0.07	2.83±0.10	2.81±0.11	4.07±1.12	3.99±1.10	3.97±1.19
16-III	2.89±0.08	2.86±0.08		4.07±1.13	4.03±1.12	
16-IV	2.96±0.08	2.93±0.05	2.91±0.11	4.18±1.18	4.13±1.16	4.11±1.16
17-I	3.12±0.41	3.09±0.42	3.06±0.45	4.38±1.33	4.34±1.32	4.31±1.32
17-II	3.06±0.40	3.03±0.41	2.98±0.40	4.28±1.27	4.24±1.26	4.19±1.25
18-I	3.21±0.39	3.19±0.40	3.17±0.40	4.48±1.36	4.44±1.35	4.42±1.34
18-V	3.31±0.87	3.54±0.86	3.24±0.88	4.44±1.35	4.40±1.33	4.36±1.34

and 13th isomers of $Si_{14}M$ for $M=Sc^-$, Ti, and V^+, respectively, with energy difference 1.43, 1.09, and 0.83 eV, and triplet-singlet energy difference 0.30, 0.20, and 0.08 eV, respectively. That structure was given by Kawamura *et al.*[18] as the third isomer of $Si_{14}Ti$.

2. $Si_{15}M$ ($M=Sc^-, Ti, V^+$)

A few low-lying energy isomers of $Si_{15}M$ are represented in Fig. 2. Structure 15-I for the ground state is similar to the ones obtained previously for the second isomer of $Si_{15}Ti$,[18] and for the third isomer of $Si_{15}Cr$.[17] The second isomer of $Si_{15}Sc^-$ and $Si_{15}Ti$ (structure 15-II) is similar to the first isomer of $Si_{15}Ti$ in Ref. 18. The second isomer of $Si_{15}V^+$ (structure 15-III, shared with the third isomer of both $Si_{15}Sc^-$ and $Si_{15}Ti$), is similar to the second isomer of $Si_{15}Cr$.[17] The structure 15-IV is formed by adding a Si atom to the lateral dimer of structure 14-I, resulting in a Si_3 unit which binds laterally to the DHP structure. That geometry resembles the sixth and eighth isomers of neutral $ZrSi_{15}$ of Ref. 19. The structure 15-V of the third isomer of $Si_{15}V^+$, which is shared with the seventh isomer of $Si_{15}Sc^-$ and the fifth isomer of $Si_{15}Ti$, was obtained previously by Kawamura *et al.*[18] as the third isomer of $Si_{15}Ti$.

The structures 15-I and 15-II remind the cubic structure of $Si_{14}Fe$[16,22] with an additional Si atom. That cubic structure was also obtained by Kawamura *et al.*[17] for the third isomer of $Si_{14}Cr$.

3. $Si_{16}M$ ($M=Sc^-, Ti, V^+$)

Several low-lying energy isomers of $Si_{16}M$ are represented in Fig. 3. For the first and second isomers of $Si_{16}M$ we obtain the structures 16-I and 16-II, and they are practically degenerate, especially for $M=V^+$. Note that structure 16-I was not found in our preliminary work[34] for $Si_{16}Sc^-$. Structures 16-I and 16-II were obtained by Kumar and co-workers[16,18] as the second and first isomers, respectively, of $Si_{16}Ti$. The structure 16-II is the Frank-Kasper (FK) polyhedron, with a nearly spherical structure and T_h symmetry.[2] It consists of a central M atom surrounded by 16 Si atoms within two closely spaced shells: one with 12 atoms (all equidistant from central), and another shell with 4 Si atoms forming a perfect tetrahedron. The structure 16-I can be seen as a distortion of the FK polyhedron (16-II), with the triangle along the threefold symmetric axis rotated by 30°. The structure 16-III can be seen as three pentagons in three parallel layers plus a capping Si atom, or, equivalently, as a pentagonal prism with the rectangular faces capped with a Si atom, plus a Si atom capping a pentagonal basis. That structure is not stable for $Si_{16}V^+$, and evolves toward the FK geometry when we take 16-III as the initial geometry of $Si_{16}V^+$. The third isomer of $Si_{16}V^+$ adopts the structure 16-IV, which is shared with the fourth isomer of $Si_{16}Sc^-$ and $Si_{16}Ti$. It coincides with the fullerenelike structure obtained previously as the third isomer of $Si_{16}Ti$,[18] and the first isomer of $Si_{16}W$.[21] The interplay between the electronic properties of $n=16$ isomers and their symmetry will be analyzed in Sec. III B 3.

4. $Si_{17}M$ ($M=Sc^-, Ti, V^+$)

A few low-lying energy isomers of $Si_{17}M$ are represented in Fig. 4. We are not aware of previous calculations reporting that type of structure, except our previous work.[34] In the structures 17-I and 17-II a dimer and a trimer, respectively, binds the lateral faces of the DHP motif. We note that the sequences of V^+ and Ti doped isomers departs considerably from the sequence for Sc^- doped clusters, and the apparent tendency towards sphericity observed for the low-lying energy isomers of $Si_{15}M$ and $Si_{16}M$ disappears.

5. $Si_{18}M$ ($M=Sc^-, Ti, V^+$)

Several low energy isomers of $Si_{18}M$ are represented in Fig. 5. The lowest energy isomer for $Si_{18}Sc^-$ and $Si_{18}Ti$ has the structure 18-I, which can be seen as a DHP structure with three silicon dimers on alternating lateral faces. Instead, the first isomer of $Si_{18}V^+$ adopts the more elongated structure 18-V. As for $Si_{17}M$ clusters, the low-lying isomers of $Si_{18}M$ departs from sphericity more than the $Si_{16}M$ and $Si_{15}M$ clusters. Thus, in the range $n=14-18$, the optimal coordination of the M impurity to Si atoms of Si_nM clusters is found for $n=15,16$.

B. Electronic properties of Si_nM clusters ($M=Sc^-, Ti, V^+$; $n=14-18$)

1. Energetics and stability

In Fig. 6 is represented, for the lowest energy isomer of Si_nM clusters, the evolution with the cluster size n of several quantities: the binding energy per atom [E_b, Eq. (1)], the addition energy of an M impurity to a Si_n cluster [E_{ad}^M, Eq. (2)], the addition energy of a Si atom to a $Si_{n-1}M$ cluster [E_{ad}^{Si}, Eq. (3)], the second difference of the total cluster energy [$\Delta_2 E_n$, Eq. (4)], and the energy difference between the LUMO and HOMO orbital eigenvalues, Δ_n^{gap}. For comparison purposes, these quantities are also represented for pure Si_n clusters. The ground state energy of pure Si_n clusters was taken from our preliminary work.[34] As a matter of fact, we have calculated again the low-lying energy isomers of Si_n and found some new isomers. In particular, for the ground state of Si_{14} we obtain a new structure with 0.07 eV lower energy than the ground state structure reported previously.[34] That new structure is similar to the second isomer of Si_{14} found by Bazterra and co-workers.[14] We can see for the various properties plotted in Fig. 6 a completely different trend with size of pure versus doped Si clusters

In panel (b) of Fig. 6 we see that $\Delta_2 E_n$ has a positive peak at $n=16$ for $M=Sc^-, Ti, V^+$, and a negative value at $n=17$. These facts, according to the usual interpretation of the cluster mass spectra,[38] indicate a high abundance of $Si_{16}M$ relative to their neighbors clusters, which agrees with the mass spectrometry experiments of Nakajima and co-workers.[31,32] In Fig. 6 we can see peaks also at $n=16$ for the binding energy per atom [panel (a)] and for the HOMO-LUMO gap [panel (c)], which can be considered additional signatures of the special stability of $Si_{16}M$ clusters. Our HOMO-LUMO gap values at $n=16$ are smaller than those found by Reveles and Khana,[33] and for the isomers 16-I to 16-III of $Si_{16}Ti$ is slightly larger than the value 1.9 eV estimated from photoelectron spectroscopy experiments.[31,32] This fact can be surprising in view of the empirically known tendency of LDA

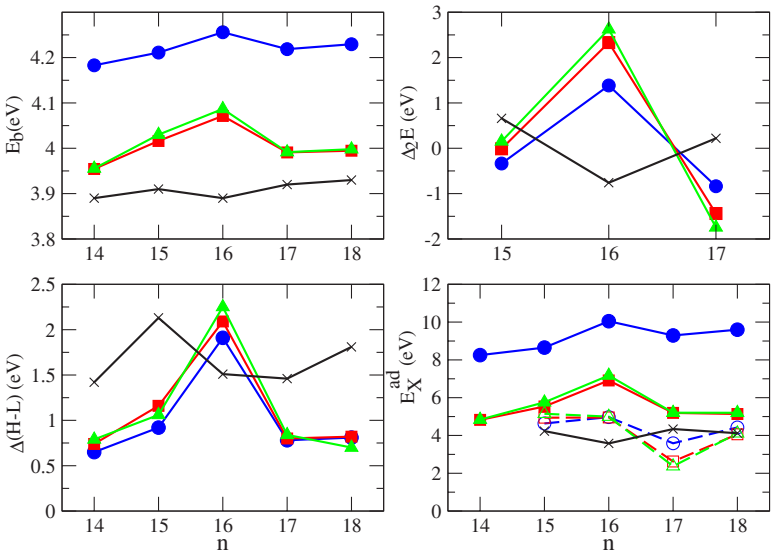

FIG. 6. (Color online) Different properties of Si_nM and Si_n clusters are represented versus the number of Si atoms n: (a) the binding energy per atom; (b) the second difference of the total energy; (c) the HOMO-LUMO gap; (d) the addition energy of M to pure Si_n clusters (filled symbols), and the addition energy of Si to doped $Si_{n-1}M$ clusters (empty symbols). Circles, squares, and triangles represent Sc^-, Ti, and V^+ doped clusters, respectively, and crosses represent pure Si_n clusters. The lines stand only to guide the eye.

and GGA calculations to underestimate the band gap of bulk semiconductors, which apparently cannot be applied to the HOMO-LUMO gap of small doped silicon clusters.

On the other hand, the addition energies of a Si atom to a pure Si_{n-1} and to a doped $Si_{n-1}M$ cluster, have comparable magnitudes but the trend with size is different, and they are systematically smaller than the addition energy of a M impurity to Si_n, as seen in panel (d) of Fig. 6.

2. Spin and charge population analysis

All structures in Figs. 1–5 correspond to spin zero, except 14-VIII of Fig. 1, which is a triplet for the three doped clusters, as was already mentioned in Sec. III A 1. For $Si_{14}V^+$ that triplet structure is near degenerate with the singlet 14-I structure.

We have investigated also the energy difference between singlet and triplet states of the isomer 16-II of $Si_{16}M$, whose equilibrium geometry is a Frank-Kasper (FK) polyhedron with spin zero: by forcing a spin 1 and relaxing the structure, we obtain equilibrium geometries which depart from the FK structure, having 1.4, 1.2, and 1.4 eV higher energy for $Si_{16}Sc^-$, $Si_{16}Ti$, and $Si_{16}V^+$, respectively.

The Mulliken population analysis of our equilibrium structures for Si_nM clusters reveals that the spin charge cancellation occurs locally, for each atom and each orbital. In the four panels of Fig. 7 is represented, for the four isomers 16-I to 16-IV of $Si_{16}M$ given in Fig. 3, the total charge accumulation and partial s-, p-, and d-orbital charge accumulation per Si atom (compared to the nominal valence of free Si atom), as a function of the radial distance to the cluster center. The radial shells are well defined for these structures, and the corresponding shell radii are smaller for V^+ than for Ti, and for Sc^- doped $Si_{16}M$. This trend was discussed above in Sec. III A.

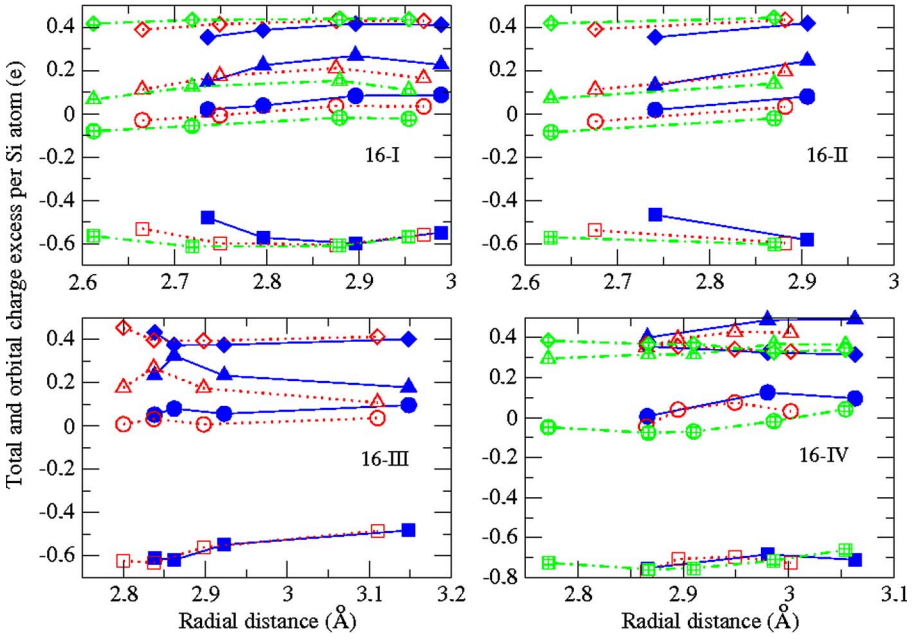

FIG. 7. (Color online) The total charge accumulation per Si atom (circles), and the s-(squares), p-(triangles), and d-orbital (rhombus) charge accumulation per Si atom, in units of one electron, are represented for $Si_{16}M$ versus the radial distance to the center of cluster. The different panels correspond to the four isomeric geometries 16-I, 16-II, 16-III, and 16-IV of Fig. 3, and the different points correspond to well defined radial atomic shells. The lines connecting points stand only to guide the eye. Filled, empty, and crossed symbols stand for Sc^-, Ti, and V^+ doped clusters, respectively.

In the isomeric geometries of $Si_{16}V^+$, the electrons flow from Si atoms to V^+ cation, whereas in the isomers of $Si_{16}Sc^-$ the electrons flow from Sc^- anion to the Si atoms, as a consequence of the relative electronegativity of these elements. The loss of *s*-orbital charge of Si atoms is larger for $Si_{16}V^+$ than for $Si_{16}Sc^-$, but the corresponding gain of *p*-orbital (*d*-orbital) charge is smaller (larger) for the cation than for the anion clusters. For $Si_{16}Ti$, it results in an intermediate situation among those for $Si_{16}Sc^-$ and $Si_{16}V^+$. From Fig. 7 we can recognize a covalent bonding for Si_nM clusters, which is more clear for Ti than for Sc^- or V^+ doped clusters. The hybridization of *s-p-d* orbitals has different weights depending on the type of impurity and geometry. For example, the *d*-orbital charge is larger than the *p*-orbital charge except for the 16-IV structure. In Sec. III B 3 below we will analyze the relation among geometry and bonding of 16-I, 16-II, 16-V, and 17-I isomers of Si_nSc^-.

The fact that the ground state geometry of $Si_{18}V^+$ differs from that of Sc^- and Ti doped clusters is due to the different electronegativity of the metal impurity relative to the Si atom, namely, Sc^- and Ti (V^+) have smaller (larger) electronegativity than Si. Thus, the V^+ cation gains 0.047 electrons per Si atom in the 18 V isomer, which is preferred to the 18-I isomer because V^+ donates 0.026 electrons per Si atom in that geometry. Contrarily, $Si_{18}Sc^-$ prefers the 18-I geometry instead of the 18-V one because the Si cage gains 0.063 electrons per Si atom in the 18-I isomer, and only 0.043 electrons per Si atom in the 18-V one.

The preference of V^+ impurity for the 17-II isomer instead of 17-I is due to a size effect, since the charge transfer among M impurity and Si cage is nearly the same for 17-I and 17-II geometries. Specifically, the amount of electrons per Si atom transferred to the Si cage in (17-I, 17-II) geometries is (0.067, 0.065) for Sc^-, (0.018, 0.018) for Ti, and (−0.037, −0.034) for V^+ doped clusters. On the other hand, the atomic radius of the impurity, already commented on in Sec. III A, correlates well with the average Si-*M* distances given in Table I, namely, 3.12 (Sc^- in 17-I), 3.09 (Ti in 17-I), and 2.98 (V^+ in 17-II). This argument cannot be applied to isomers 18-I and 18-V because the geometry 18-V departs largely from the spherical shape, and the Si-*M* average distances have a broad dispersion.

3. Symmetry and bonding: Partial density of states (PDOS)

The enhanced stability of the low-lying-energy $Si_{16}M$ species with respect to other nonspherical Si_nM isomers, is due to a special relation among the cage symmetry and the electronic structure, as discussed recently by Kumar[2] for $Si_{16}Ti$ in the context of the spherical potential model.[36,37] In that model, the orbital angular moment is a good quantum number, that is, the single particle states belong to the irreducible representations of the rotation group $O^+(3)$. For an empty cage, these states have predominantly zero radial nodes,[48] and are labeled as $1s,1p,1d,1f,1g,1h,\ldots$. The predominant covalent bonding in $Si_{16}M$, as suggested by our Mulliken population analysis, is the result of hybridization of the empty-cage states and the endohedral atom valence states having the same orbital angular moment character. This approximated *l*-selection rule was postulated for endohedral $Zr@C_{28}$ and $Zr@Si_{20}$ by Jackson and coworkers,[36,37] and is based on that only those orbitals transforming in the same irreducible representation of the point group of the endohedral complex can be mixed in a given bonding state.

The irreducible representations of the rotation group $O^+(3)$ are generally reducible in terms of the irreducible representations of its subgroups. Thus, for the T_d symmetry of the FK structure 16-II, the splitting of the monoelectronic levels in the different T_d irreducible representations is:[49] s (a_1), p (t_2), d $(e+t_2)$, f $(a_2+t_1+t_2)$, g $(a_1+e+t_1+t_2)$, h $(e+t_1+2t_2)$, $i(a_1+a_2+e+t_1+2t_2)\ldots$. This can be seen clearly in the total density of states (DOS) of $Si_{16}Sc^-$ represented in the upper panel of Fig. 8(b), where the electronic levels are grouped and then labeled according to the spherical model. In the middle and lower panels of Fig. 8(b) is shown the partial density of states (PDOS) for Sc^- atom and Si cage, and the contribution of $3d$, $4s$, and $4p$ orbitals of Sc^- to the PDOS, respectively. We see that the valence electrons of $Si_{16}Sc^-$ accommodate within the sequence of levels $1s,1p,1d,1f,2s,1g,2p,2d,1h,3s,3p,1i\ldots$ of the spherical potential model, producing a shell closing of 68 electrons when completing the orbital $2d$, which is the HOMO. This HOMO is the bonding orbital resulting from the hybridization of the $3d$ electron of Sc^- with the $2d$ $(e+t_2)$ orbital of the Si FK cage, whereas the antibonding hybrid orbital forms a part of the t_2 components of the LUMO, which is grouped in a $1h$ state of the spherical model. Similarly, the $4s$ orbital of Sc^- hybridizes with the orbital $2s$ of the FK structure, giving the bonding orbital $2s$ and the antibonding $3s$ orbital of the compound $Si_{16}Sc^-$.

An analogous analysis can be performed for the isomers 16-I and 16-III of $Si_{16}Sc^-$, both of them having D_3 symmetry. The splitting of the monoelectronic levels of O^+ (3) in the D_3 irreducible representation is:[49] $s(a_1)$, $p(a_2+e)$, $d(a_1+2e)$, $f(a_1+2a_2+2e)$, $g(2a_1+a_2+3e)$, $h(a_1+2a_2+4e)$, $i(3a_1+2a_2+4e)\ldots$. Similar quantities as in Fig. 8(b) are represented in Fig. 8(a) for the isomer 16-I of $Si_{16}Sc^-$. We see that the occupied levels of the spherical potential model, up to the HOMO level, follow the same sequence as for the FK structure 16-I, despite the fact that their splitting is different. The DOS of D_3 isomers differs from the T_d (FK) one in the sequence and/or the fine structure of the unoccupied levels of the spherical model. For 16-I, the hybridization of $4s$ of Sc^- with the part a_1 of the $1h$ of the Si cage, leads to the occupied $2s$ bonding orbital and the antibonding orbital a_1 in the LUMO $1h$ of the compound. Similarly, the bonding and antibonding orbitals formed by the hybridization of $3d$ of Sc^- and the a_1+2e part of $1h$ of the D_3 Si cage forms levels, respectively, in the HOMO and LUMO compound spherical model orbitals. This picture of the bonding of nearly spherical $Si_{16}M$ clusters is also obtained for $M=Ti,V^+$, as can be seen by inspection of Fig. 9, where it is represented the DOS, PDOS, and orbital-PDOS of structures 16-I, 16-II, and 16-IV isomers of $Si_{16}V^+$.

For nonspherically shaped clusters the bonding cannot be based on the *l*-selection rule, as can be seen by inspection of Fig. 8(c) for isomer 16-V of $Si_{16}Sc^-$, and Fig. 8(d) for isomer 17-I of $Si_{17}Sc^-$. In these figures one cannot recognize a definite symmetry, and it is clear that the $3d$ orbital of the im-

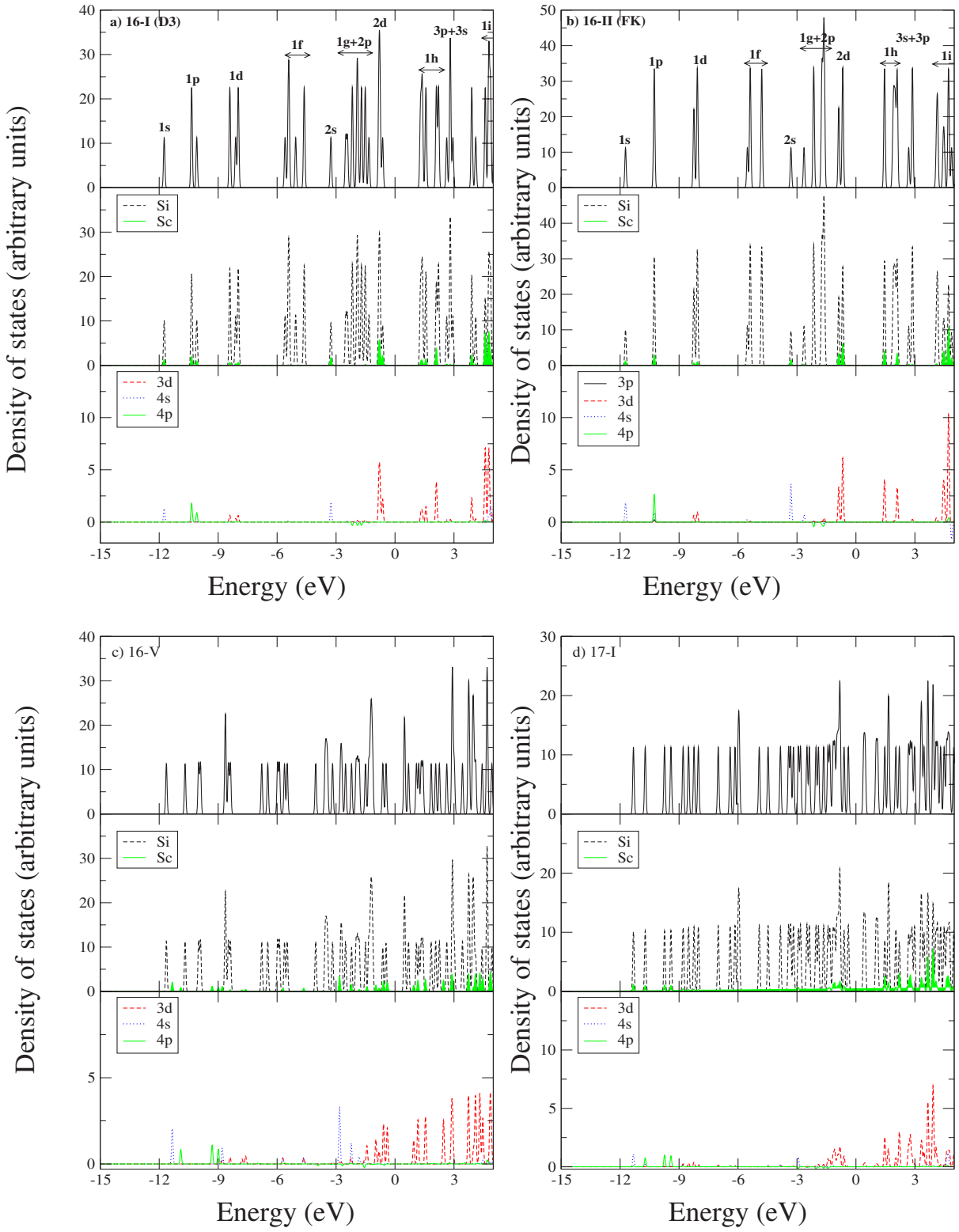

FIG. 8. (Color online) For the isomers 16-I, 16-II, 16-V of $Si_{16}Sc^-$, and 17-I of $Si_{17}Sc^-$, is shown the density of states (upper panel), the projected density of states of Sc^- (middle panel), and orbital projected density of states of Sc^- (lower panel): (a) structure 16-I; (b) 16-II; (c) 16-V; (d) 17-I. The unit in the x axis is eV, and the Fermi energy was set to zero. The splitting of the levels, which are grouped according to the labels of the spherical potential model, is caused by the different molecular symmetry of the isomers (see text).

purity is fragmented among several levels near the HOMO and, mainly, at higher energies than the HOMO. Comparing the projected density of states of the impurity in Figs. 8(c) and 8(d), with that in Figs. 8(a) and 8(b), we see that the weight of the 3d character near the HOMO level is smaller for nonspherical shaped clusters.

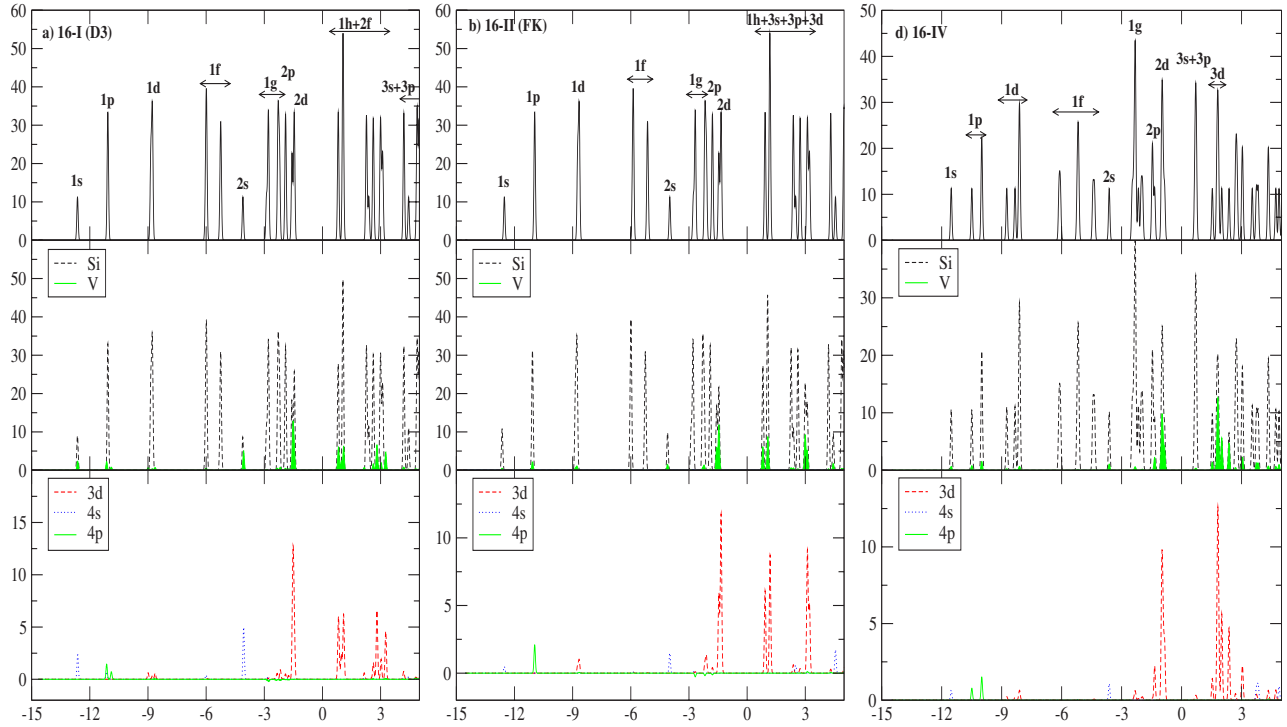

FIG. 9. (Color online) The same as in Fig. 8 for the isomers 16-I (left panels), 16-II (middle panels), and 16-IV (right panels) of $Si_{16}V^-$.

4. Electron affinity and dipole moments

In Table II is given the adiabatic electron affinity (EA_{cal}) of neutral Si_nM^0 clusters (M^0=Sc,Ti,V), calculated as the difference of total energy between neutral Si_nM^0 and anionic Si_nM^- species in its respective lowest energy state. The lowest energy state of Si_nSc, Si_nTi^-, and Si_nV^- is obtained, respectively, by relaxing several low-lying energy structures of Si_nSc^-, Si_nTi, and Si_nV^+, in which is subtracted one electron, added one electron, and added two electrons, respectively. In a second step, the lowest energy state of Si_nV is obtained by relaxing several low-lying energy structures of Si_nV^- after subtracting one electron. For $n \neq 16$ the relaxed geometries of neutral Si_nV clusters maintained the same equilibrium structures as those of initial Si_nV^- anions. For neutral $Si_{14}V$ and anionic $Si_{14}V^-$, the ground state structure is 14-VIII within doublet and singlet spin state, respectively, being 0.21 and 0.60 eV lower in total energy than structure 14-I within doublet and singlet spin state, respectively. Nevertheless, 14-I still is an equilibrium energy structure of these clusters. The energy difference between $Si_{14}V$ and $Si_{14}V^-$, when both are in the relaxed structure 14-I, is 2.67 eV, which is ~0.4 eV smaller than the adiabatic affinity reported in Table II.

TABLE II. The calculated adiabatic electron affinity (EA_{cal}, in eV) of neutral Si_nSc, Si_nTi, and Si_nV clusters. The structures of the lowest energy state for the anion and neutral species are indicated in parentheses using the labels of Figs. 1–5. For Si_nTi are also given experimental values (EA_{exp}) from Ohara *et al.*[30]

	Si_nSc	Si_nTi		Si_nV
Size	EA_{cal}	EA_{cal}	EA_{exp}	EA_{cal}
14	3.17 (I-I)	2.72 (I-I)	2.56±0.15	3.06 (VIII-VIII)
15	3.21 (I-I)	2.57 (I-I)	2.78±0.13	2.36 (I-I)
16	3.31 (I-IV)	1.88 (IV-I)	1.81±0.10	3.03 (IV-IV)
17	3.09 (I-I)	2.57 (I-I)	2.47±0.13	2.58 (II-II)
18	2.91 (I-I)	2.79 (I-I)	2.82±0.12	2.85 (V-V)

In the case n=16 we performed the above mentioned optimization process taking as initial geometries the four isomers 16-I to 16-IV of Fig. 3. We obtained for the optimized geometries of $Si_{16}Sc$, $Si_{16}Ti^-$, and $Si_{16}V^-$, the same structures as the initial ones, but within a different energetic sequence. For $Si_{16}Sc$ that sequence is just the inverse as that for $Si_{16}Sc^-$, that is, 16-IV, 16-III, 16-II, and 16-I, being 16-II slightly deformed from the FK structure, and near degenerate with 16-I. The energy difference between $Si_{16}Sc$ and $Si_{16}Sc^-$, when both are in the same (relaxed) structure, is 3.50, 3.43, 3.41, and 3.16 eV, for structures 16-I, 16-II, 16-III, and 16-IV, respectively. The difference of these values with that reported in Table II is due to the structural relaxation of $Si_{16}Sc^-$ after the loss of one electron. For $Si_{16}Ti^-$ the sequence of structures with increasing energy is 16-IV, 16-I, and 16-III, being the structure 16-II unstable and evolving towards 16-I. The energy difference between $Si_{16}Ti$ and $Si_{16}Ti^-$, when both are in the same (relaxed) structure, is 1.80, 1.89, and 2.28 eV, for structures 16-I, 16-III, and 16-IV, respectively. The difference of these values with the one reported in Table II is due to the structural relaxation of $Si_{16}Ti$ after charging with an extra electron. For $Si_{16}V^-$ the sequence of isomers with increasing energy is 16-IV, 16-I, and 16-II, being the

geometry 16-IV similar to that obtained by Reveles and Khana.[33] The structure 16-II of $Si_{16}V^-$ results to be a spin triplet. When we optimize the initial geometry 16-II of $Si_{16}V^-$ forcing a spin singlet state, it results in a different equilibrium structure at 0.45 eV higher energy than the triplet 16-II isomer. The structures of the neutral $Si_{16}V$ isomers are obtained by relaxing the structures 16-IV, 16-I, and 16-II of the anion $Si_{16}V^-$ after subtracting one electron, resulting in the same structures with the same sequence of increasing energy as the anion clusters. The energy difference between $Si_{16}V$ and $Si_{16}V^-$ in the same structure (relaxed for each cluster) is 1.97, 1.90, and 3.03 eV, for structures 16-I, 16-II, and 16-IV, respectively. We see in Fig. 3 that structure 16-IV has a smaller HOMO-LUMO gap for all impurities than 16-I, 16-II, and 16-III structures. Thus, for neutral $Si_{16}Sc$ and $Si_{16}V$ clusters within 16-IV, we obtained HOMO-LUMO gap values 0.36 and 0.65 eV, respectively, to be compared with 1.04 eV obtained for both $Si_{16}Sc^-$ and $Si_{16}V^-$. This reduction of the HOMO-LUMO gap for the neutral $Si_{16}Sc$ and $Si_{16}V$ clusters agrees qualitatively with the experimental trend obtained by Koyasu and co-workers[32] (see Fig. 6 in that reference).

We see in Table II that our results for the adiabatic electron affinities compare well with the experimental values[30] for the threshold detachment energy of Si_nTi^-, which corresponds to the upper limit of the EA of Si_nTi. Another experimental value for the adiabatic detachment energy of $Si_{16}Ti^-$, 2.03 ± 0.09, was given by Koyasu *et al.*[31,32] Two different theoretical estimations[18,33] of the EA of $Si_{16}Ti$ yield the value 1.91 eV.

The calculated vertical (adiabatic) electron affinity of $Si_{16}Sc$ is 3.56 (3.31) eV, which compare well with the experimental detachment energy[31,32] of $Si_{16}Sc^-$ 4.25 (3.41 ± 0.12) eV. The vertical affinity is obtained as the difference of energy between the neutral and anion clusters but allows relaxation of the neutral cluster within the same geometry of the anion. The experimental adiabatic detachment energy of $Si_{16}V^-$ determined recently by Koyasu *et al.*[32] is 3.08 ± 0.13 eV, which is close to our calculation, 3.03 eV, in Table II.

The HOMO-LUMO gap of $Si_{16}M$ FK (16-II) clusters calculated by Khana and Reveles[33] is 2.26, 2.34, and 2.42 eV for $Si_{16}Sc^-$, $Si_{16}Ti$, and $Si_{16}V^+$, respectively. For these FK isomers, we obtain 2.12, 2.17, and 2.25 eV, respectively. However, for the near degenerate 16-I structure of these clusters, we obtain 1.91, 2.09, and 2.25 eV, respectively. Thus, we hope that the measurement of magnitudes which are strongly dependent on the HOMO-LUMO gap, as the dipole polarizability, will allow one to discriminate the isomers 16-I and 16-II in the case of $Si_{16}Sc^-$.

In Table III is given the calculated electric dipole moment at zero temperature for the four lowest energy isomers of $Si_{16}M$ ($M=Sc^-,Ti,V^+$), and their Boltzmann weighted average at room temperature. In principle, the geometry 16-II of $Si_{16}Sc^-$ can be discriminated from the others, particularly from geometry 16-III, by means of experiments. In practice, the averaged values should be compared against experimental dipole moments at finite temperature.

TABLE III. The calculated dipole moment (Debye) for the four lowest energy isomers of $Si_{16}M$, and their Boltzmann weighted average, $\langle 16\rangle$.

	$Si_{16}Sc^-$	$Si_{16}Ti$	$Si_{16}V^+$
16-I	0.108	0.019	0.022
16-II	0.002	0.055	0.025
16-III	0.545	0.336	
16-IV	0.119	0.015	0.678
$\langle 16\rangle$	0.175	0.029	0.024

IV. CONCLUSIONS

We have studied the structural and electronic properties of the low-lying energy isomers of doped Si_nM ($M=Sc^-,Ti,V^+$) clusters in the range $n=14-18$, and we have obtained several new geometries of low-lying isomers. In particular, most of the Si_nM isomers for $n=14,17,18$, and several of the isomers for $n=15$ and 16, are here reported for the first time. The metal impurity becomes encapsulated in all cases, and the geometries have no relation to those of pure silicon clusters.[34] The lowest energy isomers of $Si_{16}M$ are nearly spherical shaped and they have smaller M-Si average distance than those clusters with neighbors sizes. This fact correlates with the higher relative stability of $Si_{16}M$ with respect to their neighbor sizes. That enhanced stability was found in experiments,[31,32] and is corroborated in this paper by means of first-principles calculations leading to positive peaks in the second difference of total energies of Si_nM clusters at $n=16$.

We have reported and discussed the trends with the cluster size of the binding energy, the addition energy of the impurity M to pure Si clusters, the adiabatic electron affinity, the HOMO-LUMO gap, and other electronic properties of these clusters, such as the charge transfer among the metal atom and the Si cage, and the dipole moments of different $Si_{16}M$ isomers. A detailed comparison of the bond properties and partial density of states is given for the few lowest energy isomers of $Si_{16}M$ clusters in the context of the spherical potential model. That study allows us to identify the interplay among geometrical and electronic factors which determine the high abundance (stability) of $Si_{16}M$ clusters detected in the experiments.

With respect to the interpretation of the experimental results in terms of the 20 electron rule by Reveles and Khana[33] or in terms of the l-selection rule,[36,37] we think that both offer complementary views, and both are based on first-principles calculations with 68 valence electrons for Si16M clusters, which is also a magic number of electrons. Our interpretation is not so drastic as that by Reveles and Khana, in the sense that these authors attach three electrons per Si atom to the Si16 cage and one electron per Si atom forms a bond with the impurity M. Instead, we insist on the combination of the 3d electrons of the impurity with d electrons of the Si cage forming a bonding orbital at the HOMO level of the cluster.

Our results for the adiabatic electron affinity of neutral species of Si_nM clusters are in very good agreement with

available experimental measurements.[31,32] We have also calculated the dipole moment of various nearly degenerate isomeric structures of $Si_{16}Sc^-$, $Si_{16}Ti$, and $Si_{16}V^+$ clusters, as well as their average values using Boltzmann weights at room temperature.

ACKNOWLEDGMENTS

We wish to acknowledge the support of the Spanish Ministry of Science (Grant No. MAT2005-03415), FEDER of the European Community, and Junta de Castilla y León (Grant No. VA068A06).

*Electronic address: begonia@ubu.es
†Electronic address: efernand@fta.uva.es
‡Electronic address: balbas@fta.uva.es

[1] K.-M. Ho, A. A. Shvartsburg, B. Pan, Z.-Y. Lu, C.-Z. Wang, J. G. Wacker, J. L. Fye, and M. F. Jarrold, Nature (London) **392**, 582 (1998).
[2] V. Kumar, Comput. Mater. Sci. **36**, 1 (2006).
[3] E. C. Honea, A. Ogura, C. A. Murray, K. Raghavachari, W. O. Sprenger, M. F. Jarrold, and W. L. Brown, Nature (London) **366**, 42 (1993).
[4] C. C. Arnold and D. M. Neumark, J. Chem. Phys. **99**, 3353 (1993).
[5] M. F. Jarrold and E. C. Honea, J. Phys. Chem. **95**, 9181 (1991).
[6] J. Muller, B. Liu, A. A. Shvartsburg, S. Ogut, J. R. Chelikowsky, K. W. Michael Siu, K.-M. Ho, and G. Gantefor, Phys. Rev. Lett. **85**, 1666 (2000).
[7] I. Rata, A. A. Shvartsburg, M. Horoi, T. Frauenheim, K. W. Michael Siu, and K. A. Jackson, Phys. Rev. Lett. **85**, 546 (2000).
[8] X. L. Zhu, X. C. Zeng, and Y. A. Lei, J. Chem. Phys. **120**, 8985 (2004).
[9] S. Yoo and X. C. Zeng, Angew. Chem., Int. Ed. **44**, 1491 (2005).
[10] S. Yoo, J. Zhao, J. Wang, and X. Zeng, J. Am. Chem. Soc. **126**, 13845 (2004).
[11] S. Goedecker, W. Hellmann, and T. Lenosky, Phys. Rev. Lett. **95**, 055501 (2005).
[12] J. Bai, L. Cui, J. Wang, S. Yoo, X. Li, J. Jellinek, C. Koehler, T. Frauenheim, L. Wang, and X. C. Zeng, J. Phys. Chem. A **110**, 908 (2006).
[13] W. Hellmann, R. G. Hennig, S. Goedecker, C. J. Umrigar, B. Delley, and T. Lenosky, Phys. Rev. B **75**, 085411 (2007).
[14] V. E. Bazterra, O. Oña, M. C. Caputo, M. B. Ferraro, P. Fuentealba, and J. C. Facelli, Phys. Rev. A **69**, 053202 (2004).
[15] O. Oña, V. E. Bazterra, M. C. Caputo, J. C. Facelli, P. Fuentealba, and M. B. Ferraro, Phys. Rev. A **73**, 053203 (2006).
[16] V. Kumar and Y. Kawazoe, Phys. Rev. Lett. **87**, 045503 (2001).
[17] H. Kawamura, V. Kumar, and Y. Kawazoe, Phys. Rev. B **70**, 245433 (2004).
[18] H. Kawamura, V. Kumar, and Y. Kawazoe, Phys. Rev. B **71**, 075423 (2005).
[19] J. Wang and J.-G. Han, J. Chem. Phys. **123**, 064306 (2005).
[20] E. N. Koukaras, C. S. Garoufalis, and A. D. Zdetsis, Phys. Rev. B **73**, 235417 (2006).
[21] J. Lu and S. Nagase, Phys. Rev. Lett. **90**, 115506 (2003).
[22] L. Ma, J. Zhao, J. Wang, B. Wang, Q. Lu, and G. Wang, Phys. Rev. B **73**, 125439 (2006).
[23] J. Wang and J.-G. Han, J. Phys. Chem. A **110**, 12670 (2006).
[24] V. Kumar, A. K. Singh, and Y. Kawazoe, Phys. Rev. B **74**, 125411 (2006).
[25] N. Uchida, T. Miyazaki, and T. Kanayama, Phys. Rev. B **74**, 205427 (2006).
[26] J. B. Jaeger, T. D. Jaeger, and M. A. Duncan, J. Phys. Chem. A **110**, 9310 (2006).
[27] S. Neukermans, X. Wang, N. Veldeman, E. Janssens, R. Silverans, and P. Lievens, Int. J. Mass. Spectrom. **252**, 145 (2006).
[28] S. M. Beck, J. Chem. Phys. **87**, 4233 (1987).
[29] S. M. Beck, J. Chem. Phys. **90**, 6306 (1989).
[30] M. Ohara, K. Koyasu, A. Nakajima, and K. Kaya, Chem. Phys. Lett. **371**, 490 (2003).
[31] K. Koyasu, M. Akutsu, M. Mitsui, and A. Nakajima, J. Am. Chem. Soc. **127**, 4998 (2005).
[32] K. Koyasu, J. Atobe, M. Akutsu, M. Mitsui, and A. Nakajima, J. Phys. Chem. A **111**, 42 (2007).
[33] J. U. Reveles and S. N. Khanna, Phys. Rev. B **74**, 035435 (2006).
[34] M. B. Torres and L. C. Balbás, European Physics J. D (to be published).
[35] H.-P. Cheng, R. S. Berry, and R. L. Whetten, Phys. Rev. B **43**, 10647 (1991).
[36] J. Jackson, E. Kaxiras, and M. R. Pederson, J. Phys. Chem. **98**, 7805 (1994).
[37] J. Jackson and B. Nellermoe, Chem. Phys. Lett. **254**, 249 (1996).
[38] C. E. Klots, J. Chem. Phys. **92**, 5864 (1988).
[39] W. Kohn and L. J. Sham, Phys. Rev. **145**, 561 (1965).
[40] J. M. Soler, E. Artacho, J. D. Gale, A. García, J. Junquera, P. Ordejón, and D. S. Portal, J. Phys.: Condens. Matter **14**, 2745 (2002).
[41] J. P. Perdew, K. Burke, and M. Ernzerhof, Phys. Rev. Lett. **77**, 3865 (1996).
[42] N. Troullier and J. L. Martíns, Phys. Rev. B **43**, 1993 (1991).
[43] L. Kleinman and D. M. Bylander, Phys. Rev. Lett. **48**, 1425 (1982).
[44] E. M. Fernández, M. B. Torres, and L. C. Balbás, Int. J. Quantum Chem. **99**, 39 (2004).
[45] M. B. Torres, E. M. Fernández, and L. C. Balbás, Phys. Rev. B **71**, 155412 (2005).
[46] Z. J. Wu and Z. M. Su, J. Chem. Phys. **124**, 184306 (2006).
[47] D. R. Lide, *CRC Handbook of Chemistry and Physics*, 79th ed. (CRC Press, Boca Raton, FL, 1999).
[48] E. M. Fernández, J. M. Soler, and L. C. Balbás, Phys. Rev. B **73**, 235433 (2006).
[49] R. F. Cotton, *Chemical Applications of Group Theory*, 2nd ed. (Wiley-Interscience, New York, 1971).